

# First Precise Spaceborne Sea Surface Altimetry With GNSS Reflected Signals

Estel Cardellach , Senior Member, IEEE, Weiqiang Li , Member, IEEE, Antonio Rius , Maximilian Semmling , Jens Wickert , Florian Zus, Christopher S. Ruf , Fellow, IEEE, and Carlo Buontempo 

**Abstract**—The precision of sea surface altimetry using bistatically reflected signals of the Global Navigation Satellite System (GNSS) is typically one to two orders of magnitude worse than dedicated radar altimeters. However, when the scattering is coherent, the electromagnetic phase of the carrier signal can be tracked, providing precise ranging measurements. Under grazing angle (GA) geometries, the conditions for coherent scattering are maximized, enabling carrier phase-delay altimetric techniques over sea waters. This work presents the first implementation of GA carrier phase sea surface altimetry using data acquired from a spaceborne platform (NASA Cyclone GNSS mission) and transmitted from both GPS and Galileo constellations. The altimetric results show that the measurement system precision is 3/4.1 cm (median/mean) at 20 Hz sampling, cm level at 1 Hz, comparable to dedicated radar altimeters. The combined precision, including systematic errors, is 16/20 cm (median/mean) precision at 50 ms integration (a few cm level at 1 Hz). The wind and wave requirements to enable coherent scattering at GA geometries appear to be below 6 m/s wind and 1.5 m significant wave height, although only 33% of tracks under these conditions present sufficient coherence. Given that this technique could be implemented by firmware updates of existing GNSS radio occultation missions, and given the large number of such missions, the study indicates that the resulting precision and spatio-temporal resolution would contribute to resolving some submesoscale ocean signals.

**Index Terms**—Carrier phase-delay altimetry, Global Navigation Satellite System (GNSS) reflectometry, grazing angle (GA) reflectometry, sea surface altimetry, submesoscale ocean altimetry.

## I. INTRODUCTION

SPACEBORNE altimetry using signals of the Global Navigation Satellite System (GNSS) reflected off the oceans (GNSS-Reflectometry or GNSS-R) has poor precision compared to dedicated radar altimeters, when GNSS-R altimetry

is conducted from small receivers using the publicly available GNSS codes, e.g., [1], [2]. This technique will be called hereafter conventional GNSS-R (cGNSS-R) and it is the one available at the NASA Cyclone Global Navigation Satellite System (CyGNSS) and U.K. TechDemoSat-1 (TDS-1) missions [3], [4]. The low precision is due to the narrow bandwidth of these GNSS codes, which limits the resolution in the domain of the signal delay or range. A way to enhance the altimetric precision is by using the wider bandwidth and encrypted codes that are transmitted for military applications. Not having access to these codes, Martín-Neira [5], [6] suggested a solution based on the use of the direct line-of-sight links as reference for the demodulation of the broad bandwidth signals in the reflected signals, a technique called interferometric GNSS-R (iGNSS-R). Several studies have analyzed theoretically and/or empirically the improvement in precision between the cGNSS-R and iGNSS-R altimetry, reporting enhancements of between two to six times in the altimetric precision obtained in 1-s integrated measurement [7]–[11]. However, the iGNSS-R technique requires more complex hardware solutions when targeting near-nadir geometries, which in addition are not suitable for very small and cheap spaceborne platforms. A way to increase the altimetric precision by one to two orders of magnitude, regardless of using iGNSS-R or cGNSS-R, and even from small and cheap receivers (e.g., suitable for nanosatellites), is by tracking the phase of the carrier electromagnetic signal of the reflected radio link. Given that GNSS works at *L*-band, around 20 cm wavelength, being able to track the carrier phase means that the altimetric delay can be measured at a few cm level in a few millisecond sampling intervals. For example, from spacecraft platforms this has been achieved over ice sheets [12], sea ice [12], [13], and lakes [14]. We will call this technique carrier phase-delay altimetry, or *carrier phase altimetry* (CaPA) for short. Carrier phase-delay altimetry is only possible when the reflection is dominated by coherent scattering, otherwise the diffuse component adds randomlike behavior to the carrier phase, from which the delay cannot be further retrieved. Unfortunately, most reflections off the ocean surface follow a diffuse scattering mechanism hindering the tracking of the carrier signals. Exceptions are observations over very calm ocean surface conditions or under very slant geometries [12]–[14]. The latter condition holds because the actual roughness observed at very high incidence angles is effectively reduced. Simulations reported that altimetric retrievals using signal carrier information are limited, under such grazing conditions, to significant wave heights (SWHs) on the

Manuscript received August 30, 2019; revised October 17, 2019 and November 4, 2019; accepted November 5, 2019. Date of publication December 29, 2019; date of current version February 12, 2020. The work conducted at ICE-CSIC/IEEC was supported by Spanish Grant RTI2018-099008-B-C22 (MCIU/AEI/FEDER, UE). (Corresponding author: Estel Cardellach.)

E. Cardellach, W. Li, and A. Rius are with the Institute of Space Sciences (ICE-CSIC), 08193 Barcelona, Spain, and also with the Institute of Space Studies of Catalonia, 08034 Barcelona, Spain (e-mail: estel@ice.csic.es; weiqiang@ice.csic.es; rius@ieec.uab.es).

M. Semmling, J. Wickert, and F. Zus are with the GeoForschungsZentrum, 14473 Potsdam, Germany (e-mail: maxsem@gfz-potsdam.de; wickert@gfz-potsdam.de; zusflo@gfz-potsdam.de).

C. S. Ruf is with the University of Michigan, Ann Arbor, MI 48109-2143 USA (e-mail: cruf@umich.edu).

C. Buontempo is with the European Centre for Medium-Range Weather Forecasts, Reading RG2 9AX, U.K. (e-mail: carlo.buontempo@ecmwf.int).

Digital Object Identifier 10.1109/JSTARS.2019.2952694

sea surface  $< 1.2$  m [15]. We call the latter measurements *grazing angle (GA) carrier phase altimetry (GA CaPA)*. In total, 70% of the GNSS radio occultation (RO) atmospheric soundings occurring over the oceans unintentionally present coherent ocean reflected signals [16]. However, these reflections correspond to geometries nearly tangent to the surface, not suitable for altimetric, i.e., vertical, retrievals [17]. In [18], data acquired from 3500 m altitude flights over open sea waters showed it is optimal to obtain coherent scattering of GNSS signals and perform its corresponding phase-delay altimetry in grazing geometries between  $\sim 5^\circ$  and  $30^\circ$  elevation angle ( $60^\circ$ – $85^\circ$  incidence). These studies are promising, but conducted at slow speeds and low altitude compared to spaceborne scenarios. Dedicated studies are required to prove the feasibility of GA CaPA from space, which is the goal of the study presented in the following. This is also of interest considering the current development of ESA PRETTY mission, which will attempt GA altimetry<sup>1</sup>.

The main impairment to conduct this type of study is the acquisition of the spaceborne data, as currently the GNSS-R missions in orbit point their antennas to angles closer to nadir, away from the grazing geometries. Despite this restriction, we have reprocessed existing NASA CyGNSS mission raw data samples to search for GA reflected signals at the edge of the antenna pattern, and assess whether GA CaPA is possible from space.

## II. DATASETS AND PROCESSING

The CyGNSS mission is a constellation of eight microsats,  $< 30$  kg each, that take near-nadir GNSS-R observations for wind speed measurements. CyGNSS main objective is to improve hurricane forecasting by better understanding the interactions between the sea and the air near the core of a storm [3]. The satellites are orbiting at low altitude ( $\sim 514$  km) around central latitudes ( $35^\circ$  orbit inclination), since December 15, 2016. We present the analysis of 63 tracks of GNSS signals reflected off the sea surface in GA geometries, captured in raw mode by the NASA's CyGNSS spacecraft constellation in the Central American region. This is the region with the largest number of CyGNSS *raw acquisition* samples. The *raw acquisition* is a mode of operation for which the receiver aboard only down-converts and samples the antennas' voltages without any tracking or demodulation of the transmitted signal structure. The data, sampled at 16.0362 MHz, are then downlinked to the ground, where the researchers can process them by means of flexible software receivers, in laboratory computers. Because of the large volume of data generated every second under raw acquisition mode, these operations can only be activated during short periods of time, typically 1 min, sporadically and for dedicated studies only.

The data analyzed in this study focus on raw acquisitions over sea water acquired during 24 different days, one to a few minutes each day, corresponding to the periods September–October 2017 and September–October 2018. The acquisitions cluster in groups of two to three days, mainly coincident with the presence of

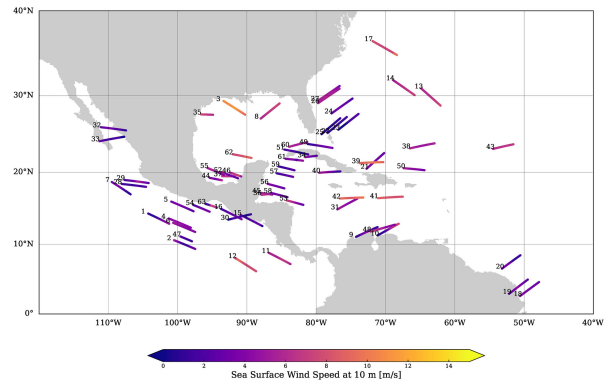


Fig. 1. Map of the location of the 63 GA GNSS-R tracks found in the CyGNSS raw data samples around Central America, wind condition in the color scale; the numbers identify the tracks in Table II of Appendix A.

tropical cyclones around the antennas' main footprint. The proximity of hurricanes within several hundred kilometer of the reflected tracks under analysis may have enhanced the long wave portion of the sea state along the tracks. The map with the location of the specular points of the reflected signals (hereafter called tracks) is shown in Fig. 1, with indication of the collocated ERA-5 wind speed [19]. Table II in Appendix A lists the tracks, identifies the receiving CyGNSS satellite, the transmitting GNSS, the date of the acquisition and several aspects of the surface conditions, according to the ERA-5 products. Note that, despite the data were mostly acquired during hurricanes occurring below the receiving satellite, the GA tracks are away ( $> 1000$  km) from its nadir ground track, therefore, the range of wind speeds found in this set does not exceed 11 m/s.

The processing of the sets has followed the same steps as in other TDS-1 and CyGNSS raw acquisition phase-delay altimetry studies, such as [13], [14]. The raw data samples are cross-correlated against synthetic replicas of the signal, generated by the software receiver, and for which both the delay and Doppler effects must be compensated to obtain above-noise correlation. We used 50 ms coherent integration time, which corresponds to along-track sampling resolutions of  $\sim 400$  m. The actual spatial resolution is a combination of this sampling value and the size and orientation of the Fresnel zone. Typically, the first Fresnel zone at GAs expands 1–2 km in the scattering plane direction and  $\sim 400$  m in the orthogonal one. The peak of the correlation function informs about the residual delay and Doppler of the signal, with respect to the ones used in the synthetic replica (also called “open-loop” model). The final measured range is reconstructed combining the information used in the model and the residual phase value. The readers are pointed to these articles for details of the processing and altimetric inversion chain, which requires tropospheric and ionospheric information to generate atmospheric corrections. ERA-5 and GIM models have been used, respectively [19], [20]. As in these previous studies, the altimetric retrievals shown here are not absolute, but relative altimetric tracks with an offset adjusted to fit the DTU18 mean sea surface (MSS) height. Combination with pseudorange (group delay observables) ranging measurements could yield to absolute altimetry, not discussed in this study.

<sup>1</sup>[Online]. Available: [http://www.esa.int/Our\\_Activities/Space\\_Engineering\\_Technology/Technology\\_CubeSats](http://www.esa.int/Our_Activities/Space_Engineering_Technology/Technology_CubeSats)

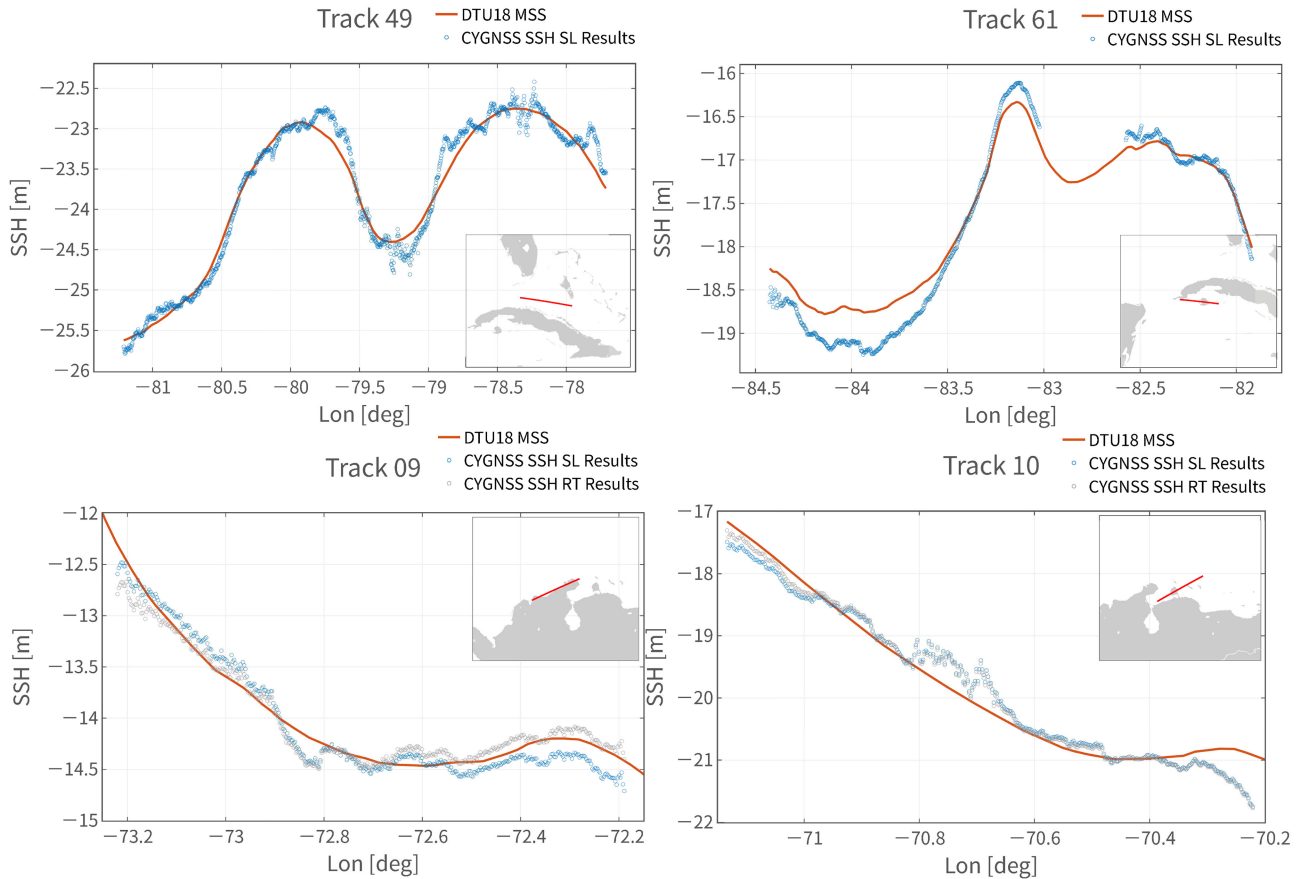


Fig. 2. Top-left: Altimetric results (circles) obtained from CyGNSS spacecraft 01 data every 50 ms (no further filtering) along a track of GPS PRN15 acquired on September 15, 2018, at  $\sim 17.5^\circ$  elevation angle over a zone with  $\sim 4.6$  m/s wind and  $\sim 0.4$  m SWH, and corrected under straight-line propagation assumption. The MSS height from DTU18 is shown as a red solid line. Top-right: Same for CyGNSS spacecraft 05 receiver and Galileo PRN05 transmitter on October 14, 2018, at  $\sim 13.4^\circ$  elevation angle over  $\sim 4.3$  m/s wind and  $\sim 0.7$  m SWH. Bottom-left: Same for CyGNSS spacecraft 04 receiver and Galileo PRN18 transmitter acquired on September 8, 2017, at  $\sim 14.7^\circ$  elevation angle over a zone with  $\sim 3.3$  m/s wind and  $\sim 0.5$  m SWH. Blue and gray dots correspond to atmospheric corrections computed assuming straight-line propagation or bending of the rays, respectively. Bottom-right: Same for GPS PRN12 acquired from the same CyGNSS acquisition, at  $\sim 13.1^\circ$  elevation angle over  $\sim 4.4$  m/s wind and  $\sim 0.7$  m SWH.

At GA geometries, the effect of the atmospheric vertical gradients can be sufficient to bend the rays, increasing the total range or delay measurement. In case of a bent radio link, the altimetric retrieval would be better performed by means of ray-tracers, as suggested for GA altimetry aboard GEROS-ISS and G-TERN [21], [22] and implemented in the airborne studies [18]. In this article, both straight-line and ray traced bent propagations have been considered.

### III. RESULTS

Fig. 2 (top) shows two of the altimetric retrievals, one using GPS signals and the other using Galileo signals, corrected for tropospheric and ionospheric effects assuming straight-line propagation. The retrievals, provided every 50 ms without any further smoothing or filtering, are compared to the DTU18 MSS height. The results show 1) little noise levels (generally around or below decimeter level at 50 ms integration), 2) good general fit with the MSS model, and 3) some slow-varying residual misfits. Here *slow varying* refers to dynamics significantly slower than the 20 Hz retrievals, so not induced by thermal noise of the range

measurements. The slow-varying residuals are expected in this analysis, because the tropospheric and ionospheric corrections applied are very simple, and other aspects of the mission relevant to the altimetric inversion are not fully solved (e.g., precise orbit determination, clock errors, precise platform and antennas attitude, etc.). Note that these mission related limitations would not be a problem with a dedicated GA CaPA mission designed to measure ocean altimetry.

To assess the impact of the bending of the rays in both the receiver operations and the altimetric retrievals, Fig. 2 (bottom) shows the altimetry along two more reflected tracks, also from both Galileo and GPS signals. In these cases, we present the retrievals using straight-line propagation corrections (as in Fig. 2-top) together with bent propagation corrections. These corrections are performed using a ray tracer [23], with ERA-5 temperature, pressure, and humidity input [19] and IRI ionospheric information [24]. A similar approach was used in the processing of the airborne campaign data [18]. The analysis of the differences between the straight-line and bent propagation corrections shows that the differences are sufficiently small, so a receiver could neglect the bending effects. This means that



TABLE I  
DISPERSION OF THE ALTIMETRIC RESULTS ATTRIBUTED TO THE MEASUREMENT SYSTEM ITSELF,  $^{ms}$ , OR ALL COMBINED EFFECTS

Track ID	$\sigma_{20\text{Hz}}^{ms}$ (cm)	$\sigma_{1s}^{ms}$ (cm)	$\sigma_{20\text{Hz}}$ (cm)	$\sigma_{1s}$ (cm)
9	2.5 (2.5)	0.6 (0.6)	13 (11)	2.9 (2.5)
10	4.8 (4.8)	1.1 (1.1)	27 (24)	6 (5.4)
18	3.0	0.7	9	2
22	1.6	0.4	9	2
25	2.3	0.5	39	8.7
31	7.2	1.6	38	8.5
44	8.3	1.9	16	3.6
45	4.7	1.0	30	6.7
49	3.3	0.7	15	3.4
51	3.0	0.7	16	3.6
53	6.6	1.5	15	3.4
61	1.8	0.4	21	4.7

Tides have not been corrected. The two cases in brackets correspond to the inversion using ray tracers, to account for bent propagation. The third and last columns include the 1-s integration equivalent precision for the measurement system and combined solutions,  $\sigma_{1s}^{ms}$  and  $\sigma_{1s}$ , respectively.

receivers onboard satellites would not need to implement ray tracer based corrections to properly track the signals. However, as it can be seen in Fig. 2 (bottom-left), the retrievals can be rather different, especially at very low elevation angles, and therefore ray tracer approaches would be generally required for proper retrieval algorithms. These retrieval schemes could be implemented on the ground, in postprocessing.

With the available retrieved tracks, a preliminary precision figure can be given. It is preliminary because of the limited amount of tracks, geographical location, seasonal occurrence (September–October during hurricanes life), the simplicity of the corrections applied, the lack of some of them (clock errors, residual precise orbit determination, tides, roughness effects, etc.), and the generally low gain of the CyGNSS receiving antenna when pointing to GA geometries. Therefore, the precision figures of the altimetric retrievals correspond, in fact, to a mixture of two kinds of errors: random noise and remaining systematic effects. The former is due to limitations of the measurement system itself, triggered by thermal noise and speckle, to which we refer as *measurement system* error hereafter, as in, e.g., [25]. The latter includes uncertainty and errors in modeling and corrections, some of which could be better solved in other or dedicated missions.

We identify the measurement system contribution,  $^{ms}$ , through the root-mean-square error (RMSE) between the 20-Hz CyGNSS solution and a 1-s sliding window smoothed one,  $\sigma_{20\text{Hz}}^{ms}$ . It captures the measurement system precision on the time scale of the thermal and speckle noise (10 s of milliseconds) by subtracting a filtered version that has been smoothed by a much longer (1 s) running average. The measurement system precision at 20 Hz, obtained for each track, is presented in Table I, with values between 1.6 and 8.3 cm, a mean of 4.1 cm, and 3.0 cm median. The measurement system contribution to the precision budget would be further reduced with longer integration intervals, e.g., cm level after 1 s integration ( $\sigma_{1s}^{ms} = \sigma_{20\text{Hz}}^{ms}/\sqrt{20}$ ). These precision levels correspond to the limit of the technique, should all systematic effects be properly corrected.

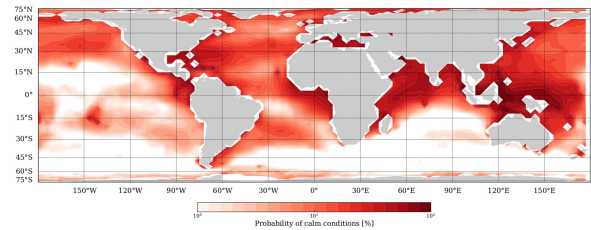


Fig. 3. Global map showing the probability of calm conditions, understood as percentage of time during which the required calm conditions apply, computed along one year time span. Plot generated with C3S CDS Toolbox. The Toolbox code is provided in Appendix C.

To take into account the other effects that reduce precision, the RMSE between our 20-Hz CyGNSS solutions and DTU18 MSS,  $\sigma_{20\text{Hz}}$ , is also compiled in Table I. It takes values between 9 and 39 cm at 50 ms integration, a median value of 16 and 20 cm mean. These values are significantly larger than the measurement system contribution for a given integration time, an indication that the systematic effects are predominant in the data processing. This is expected because of the simplicity of the corrections applied and the lack of some of them. Their 1-s integration equivalent precision  $\sigma_{1s} = \sigma_{20\text{Hz}}/\sqrt{20}$ , assuming uncorrelated 20-Hz noise, lays between 2 and 8.7 cm, with 3.6 cm median and 4.5 cm mean. Note that the RMSE errors at 20 Hz used to compute  $\sigma_{1s}$  include correlated errors. This has two competing effects on the interpretation of  $\sigma_{1s}$ : on the one hand, averaging to 1 s would not reduce the error as much as in uncorrelated noise (too optimistic  $\sigma_{1s}$  in Table I), whereas on the other hand, the major correlated residual effects are likely to be corrected in a dedicated mission or improved analysis (ionosphere, orbits, clocks, tides); hence, the actual 20-Hz precision figures are finer than the ones presented in Table I (thus finer  $\sigma_{1s}$  also expected). The along-track resolution of 1-s integrated solutions is  $\sim 7\text{--}8$  km.

#### IV. COHERENCE OF THE SIGNALS

The results presented above and in Appendix B compile retrievals from the only 12 tracks out of 63, for which the reflected signals present coherence (20%). Comparing the characteristics of the coherent and diffuse tracks, compiled in Table II of Appendix A, one notices that all the coherent tracks respond to antenna gains above  $-15$  dB, elevation angles below  $25^\circ$ , wind speeds up to 6 m/s, SWH below 1.5 m, surface mean square slopes below 0.004, and waves' steepness up to 0.021. We could not find any correlation between coherence and the orientation of the waves with respect to the scattering plane, but most of the coherent tracks occurred during local daytime, with a few exceptions, which could indicate ionospheric scintillation problems in some of the diffuse tracks. Because of the limited amount of data, these *required conditions* are only preliminary, and perhaps particular to the geographic location and seasonal moment of the acquisitions.

The required conditions are not sufficient. Among the 63 GA tracks, 36 of them fulfill the required conditions but only

TABLE II  
IDENTIFICATION OF THE 63 TRACKS PROCESSED IN THIS ANALYSIS

ID	Coh.	Elev.	Gr	U10	SWH	MSS	Lon.	Lat.	Date	GNSS	PRN	CyGNSS
1	0	19.43	6.56	3.15	1.3	0.002	-101.21	12.89	20170825	G	2	4
2	0	14.12	-2	2.75	1.5	0.002	-97.45	9.33	20170825	E	3	4
3	0	25.61	7.36	11.05	2.33	0.012	-90.25	27.6	20170825	G	1	4
4	0	13.1	3.61	5.04	1.28	0.002	-98.08	12.33	20170825	E	3	6
5	0	13.43	4.61	3.94	1.17	0.002	-97.7	14.64	20170825	E	3	7
6	0	13.02	3.18	4.84	1.29	0.002	-97.46	11.74	20170825	E	3	8
7	0	10.9	-13.14	3.19	1.33	0.002	-106.78	16.99	20170825	E	8	8
8	0	17.13	-7.56	7.34	1.11	0.006	-85.29	29.02	20170908	G	4	4
9	1	14.76	3.71	3.29	0.5	0.001	-71.14	12.42	20170908	E	18	4
10	1	13.19	3.76	4.36	0.74	0.003	-68.1	12.89	20170908	G	12	4
11	0	6.52	11.09	5.33	1.54	0.005	-83.72	7.17	20170909	E	14	1
12	0	2	9.14	8.41	1.87	0.009	-88.67	6.14	20170909	E	26	1
13	0	12.36	-18.32	7	2.02	0.006	-62.06	28.74	20170909	E	2	1
14	0	16.01	-10.9	6.3	2.3	0.006	-65.81	30.07	20170909	G	29	1
15	0	5.57	-0.04	2.55	1.29	0.002	-87.77	12.56	20170910	E	22	6
16	0	4.15	-3.88	2.31	1.35	0.001	-90.76	13.52	20170910	E	30	6
17	0	17.28	4.47	8.45	1.88	0.009	-68.36	34.94	20170910	G	25	6
18	1	11.5	3.46	3.72	1.45	0.002	-47.85	4.59	20170919	G	7	1
19	0	10.16	2.35	3.84	1.36	0.002	-49.46	4.95	20170919	G	7	3
20	0	8.55	-0.27	2.7	1.49	0.002	-50.54	8.43	20170919	E	18	6
21	0	15.52	-0.97	3.86	1.19	0.001	-70.19	22.58	20170919	E	24	7
22	1	12.83	1.91	2.1	1.3	0	-75.58	27.29	20170920	E	1	6
23	0	8.91	2.07	2.05	2.01	0.001	-73.9	27.69	20170920	E	1	7
24	0	13.44	3.47	3.47	2.2	0.001	-74.76	29.63	20170920	G	25	8
25	1	14.42	-0.46	2	0.81	0	-76.53	27.13	20170920	E	1	8
26	0	18.07	3.99	5.97	1.38	0.003	-76.63	30.87	20170921	G	25	4
27	0	12.4	3.33	5.77	1.36	0.003	-76.62	31.19	20170921	G	25	8
28	0	9.63	2.44	2.27	2.12	0.001	-104.55	18.01	20171007	G	15	3
29	0	11.13	2.3	3.71	2.11	0.002	-104.17	18.54	20171007	G	15	7
30	0	8.59	-1.91	2.14	1.95	0.001	-89.41	14.21	20171008	E	9	1
31	1	8.89	-4.59	4.96	0.88	0.003	-74.06	16.39	20171008	E	1	8
32	0	23.54	-4.25	3.18	0.55	0.002	-107.43	25.56	20171230	G	22	8
33	0	18.73	5.35	2.54	0.61	0.001	-107.69	24.74	20180303	G	16	5
34	0	10.03	1.81	4.2	0.46	0.001	-79.9	22.23	20180821	B	30	6
35	0	20.54	0.43	7.29	0.87	0.005	-94.88	27.58	20180821	E	27	6
36	0	5.06	10.99	7.27	1.05	0.006	-86.07	17.09	20180822	B	27	3
37	0	8.28	10.43	6.77	0.78	0.005	-91.77	19.45	20180823	E	18	7
38	0	17.55	12.36	5.73	1.26	0.004	-62.93	23.87	20180827	G	25	1
39	0	12.19	6.61	9.46	1.36	0.009	-70.32	21.37	20180827	B	30	1
40	0	6.82	-21.89	4.27	0.65	0.002	-76.5	20.12	20180827	G	31	1
41	0	5.69	9.69	8.58	1.35	0.008	-67.51	16.66	20180827	G	29	1
42	0	4.26	2.77	9.2	1.87	0.009	-73.21	16.55	20180827	E	27	1
43	0	7.08	-7.56	6.88	1.2	0.005	-51.55	23.74	20180827	G	5	1
44	1	9.66	2.35	4.72	0.6	0.002	-93.62	18.92	20180905	G	31	1
45	1	7.92	-0.73	6.18	0.87	0.004	-86.34	16.94	20180905	G	29	1
46	0	21.47	7.24	7.01	0.52	0.003	-90.81	19.43	20180907	G	31	2
47	0	2.31	0.39	2.08	1.76	0.002	-97.93	10.41	20180907	G	26	2
48	0	1.98	1.05	5.03	0.83	0.003	-68.61	12.76	20180913	E	21	2
49	1	17.5	5.28	3.48	0.45	0.001	-77.65	23.26	20180915	G	15	1
50	0	8.15	-2.96	5.08	2.42	0.004	-64.38	20.28	20180915	G	17	1
51	1	13	0.08	2.46	0.21	0	-81.15	22.4	20180915	E	8	1
52	0	15.11	2.46	4.39	0.66	0.003	-91.28	19.19	20181011	G	17	7
53	1	12.38	-7.43	5.31	0.6	0.003	-81.86	15.53	20181011	E	5	7
54	0	11.44	3.04	3.73	1.75	0.003	-95.37	14.58	20181012	B	30	6
55	0	24.08	5.81	5.69	0.99	0.003	-93.33	19.63	20181012	G	17	6
56	0	15.13	-8.01	3.95	0.63	0.001	-84.6	17.81	20181013	E	7	4
57	0	18.09	-7.54	2.82	0.6	0.001	-83.33	19.38	20181013	G	1	4
58	0	13.15	-9.06	3.84	0.61	0.001	-84.15	16.59	20181013	E	7	8
59	0	20.94	-4.56	2.25	0.55	0.001	-83.13	20.27	20181013	G	1	8
60	0	20.15	6.05	5.52	0.68	0.003	-81.28	24.02	20181014	G	4	1
61	1	13.42	-8.29	4.08	0.36	0.001	-81.91	21.56	20181014	E	5	5
62	0	14.86	4.72	8.41	1	0.007	-89.34	21.93	20181014	G	22	5
63	0	9.3	-9.31	4.83	1.25	0.004	-94.33	15.17	20181102	B	24	6

The different columns relate to: Track ID, coherence (1 for coherence found, 0 otherwise), elevation angle at the specular point (deg), CyGNSS receiver antenna gain at the direction of the specular point (dB), average wind speed along the track (m/s, from ERA-5 interpolation), SWH averaged along the track (m, from ERA-5 interpolation), mean slope square (MSS) of the surface waves (ADIM, from ERA-5 interpolation), longitude E averaged along the track (deg), latitude N averaged along the track (deg), date YYYYMMDD, GNSS constellation (G = GPS, E = Galileo, B = BeiDou3), GNSS transmitter PRN number and CyGNSS LEO spacecraft number.

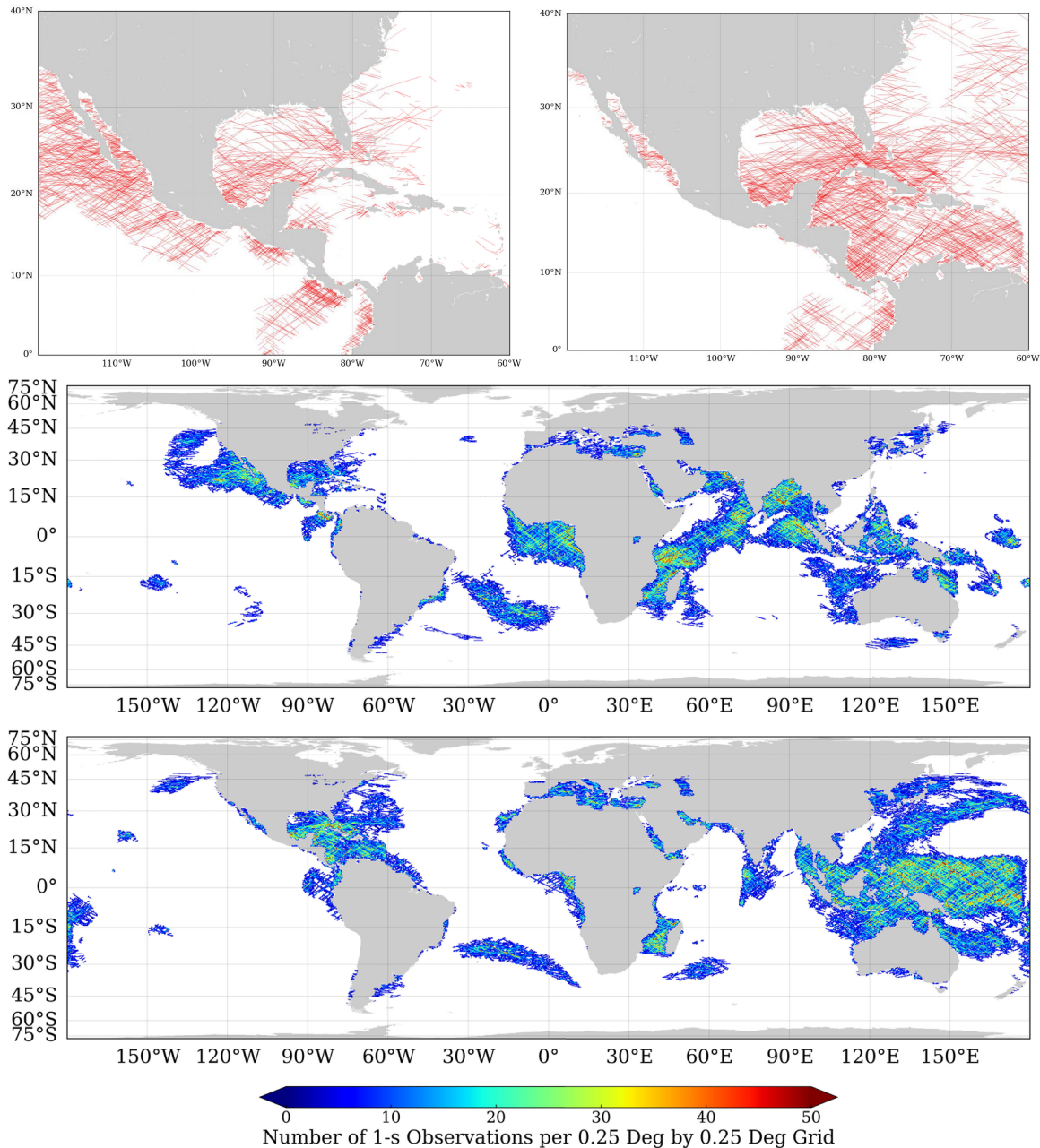


Fig. 4. Top-left: Simulation of the potential coverage during three days (February 1–3, 2018), using a CyGNSS-like constellation capable to track GA CaPA between  $10^\circ$  and  $20^\circ$  elevation angles from GPS, Galileo, GLONASS and BeiDou, and collocated with ERA-5 wind and waves products. The tracks correspond to randomly picked 33% of those under the required wind and wave conditions. Top-right: Same for the period October 11–13, 2018. Center: Number of 1-s observations in a grid of  $0.25^\circ \times 0.25^\circ$  cells across the global oceans, during the three-days period of February 1–3, 2018 (only 33% of those under the required wind and wave conditions have been considered). Bottom: Same for the October 11–13, 2018, period.

12 result in coherent signals (33%). It is not clear if this percentage will prevail in other regions and seasons, so it is a preliminary number. It is also unclear if it could be improved with smarter processing techniques. In fact, at this stage we do not have sufficient data to hypothesize about the coherence and lack of coherence under the same surface conditions, and it could also be unrelated to the surface itself. For instance, perhaps the 12 coherent tracks were captured through secondary lobes of the antenna, of higher gain than the nominal ones reported in the paragraph above, or they could be the only ones under

stable ionospheric conditions (no scintillation). Answering these question will require larger amounts of data, not available at the moment.

## V. DISCUSSION

Assuming that these preliminary findings prevail, what would be the potential use of precise altimetric retrievals in only  $\sim 33\%$  of the relatively calm scenarios imposed by the *required conditions*? To answer this question, we have inferred the percentage



of time during which the required conditions hold across the globe, over cells of  $0.75^\circ \times 0.75^\circ$ , from ERA-5 hourly gridded reanalysis products provided by the Copernicus Climate Change Service (C3S) Climate Data Store (CDS) [19] (see Fig. 3). To illustrate the effects of the 33% reduction into the spatial resolution, we have simulated the GA tracks that a CyGNSS-like constellation would acquire if it were modified to routinely collect GA reflected signals from GPS, Galileo, GLONASS, and BeiDou GNSS constellations between  $10^\circ$  and  $20^\circ$  elevation angles. Two batches of three days each have been simulated, for two different seasons. After colocating all the tracks with ERA-5 wind and wave products, only those tracks occurring under the required conditions are kept, and finally, 33% of them are randomly selected to show the expected spatial coverage in three days temporal resolution. As shown in Fig. 4, the examples from both seasons present a dense mesh of potential altimetric tracks in three days, sufficiently dense to resolve some submesoscale sea surface signals. These figures suggest that CaPA GA retrievals could successfully monitor a diversity of areas on the globe. This fact, added to the fine precision figures, makes this technique suitable to study some submesoscale sea surface phenomena. Furthermore, submesoscale features emerge or are magnified under calm conditions, especially just after a wind event has stirred the upper ocean, when the Ekman circulation interacts with the underlying mesoscale turbulence resulting in rich submesoscale structures. A special case of interest would be the study of hurricane wakes, which last several days after the pass of the cyclone [26].

Moreover, GNSS RO missions could easily be upgraded to track these types of reflected signals, without need to modify their hardware subsystems. This would require an extension of the open-loop receiver models to account for the dynamics of the reflected signals, through firmware uploads, which is simple to implement. Additionally, data storage and downlink capabilities, and other relevant system specifications should be updated to avoid loss of RO or GA CaPA data. There are currently over 16 satellites in orbit that operate GNSS RO payloads, supported by national or international agencies (e.g., USA/Taiwan COSMIC and COSMIC-2, EUMETSAT Metop-A to Metop-C, China FY3, Germany TerraSAR, TandemX, USA/Germany GRACE-FO, Spain PAZ, etc.), and tens of private commercial ones. This scenario provides a very dense spatio-temporal coverage of potentially precise phase-delay altimetry, with the advantages of: 1) already working at two frequencies for better ionospheric corrections; 2) near-real time download—short latency for numerical models and operations; and 3) long-term plans to expand and maintain large number of such satellites.

## VI. CONCLUSION

This study has presented the first GA carrier phase-delay sea surface altimetric retrievals up to  $25^\circ$  elevation angle from spaceborne platforms, resulting in a measurement system precision of 3–4 cm at 20 Hz sampling, a centimeter level with 1 s integration, despite the fact that the signals were received away from the antenna main beam. The combined precision figure

takes values between 9 and 39 cm (16 cm median, 20 cm mean) in 50 ms integration time, mostly driven by residual systematic errors due to simple or missing corrections. This precision level could scale down to a few cm level after 1 s integration, with typically 7–8 km along-track spatial resolution. The measurement system component of the precision is similar to those obtained with dedicated monostatic radar altimeters, e.g., [27]. However, further investigation is required to test the potential correction of the different error contributions, especially because GA CaPA tracks do not repeat, a fact upon which some of the radar altimeter corrections rely. This could degrade the final accuracy achievable by the GA CaPA technique, despite its high measurement system precision.

Over sea water, this precision level is unprecedented in spaceborne GNSS-R, for which it was only achieved over smoother surfaces such as sea ice [13] and lakes [14]. It is also noted that it has been achieved using both GPS and Galileo transmitted signals. The analysis seems to indicate that this technique can be applied only under certain water surface conditions, relatively calm ( $<6$  m/s wind,  $<1.5$  m waves). These are required but not sufficient conditions, as only a third of the tracks under these calm scenarios do finally present sufficient coherence to proceed with the CaPA measurements. Why tracks under the same conditions might present or lack coherence? The limited amount of data available at the moment, mostly focused on one geographical area, hurricane season and daytime events, makes it difficult to investigate. The fact that the CyGNSS antennas do not point toward GA geometries might also have negative impact. Nevertheless, even if only 33% of the tracks acquired under the calm conditions could finally be usable, the spatio-temporal coverage of a CyGNSS-like mission prepared for GA CaPA measurements would have potential to study some submesoscale sea phenomena in a diversity of areas on the earth. Moreover, it would be technologically possible to implement this technique in GNSS RO missions, opening the way to combined atmospheric GNSS RO plus altimetric GNSS-R dual frequency measurements, with unprecedented spatio-temporal resolution for sea surface altimetric measurements, thus complementing monostatic radar altimetric Flagship Missions.

## APPENDIX A TRACKS INFORMATION

Table II lists the 63 GNSS-R tracks found in raw CyGNSS data around the Central American region under GA geometry.

## APPENDIX B ALTIMETRIC SOLUTIONS

The rest of altimetric GA CaPA solutions as obtained at 50 ms integration time using CyGNSS raw data are shown in Figs. 5 and 6 (circles), together with the DTU18 MSS height (solid lines). The title of each plot includes the track ID and the RMSE error with respect to DTU18 for each particular track, at 50 ms integration ( $\sigma_{20\text{Hz}}$ ).

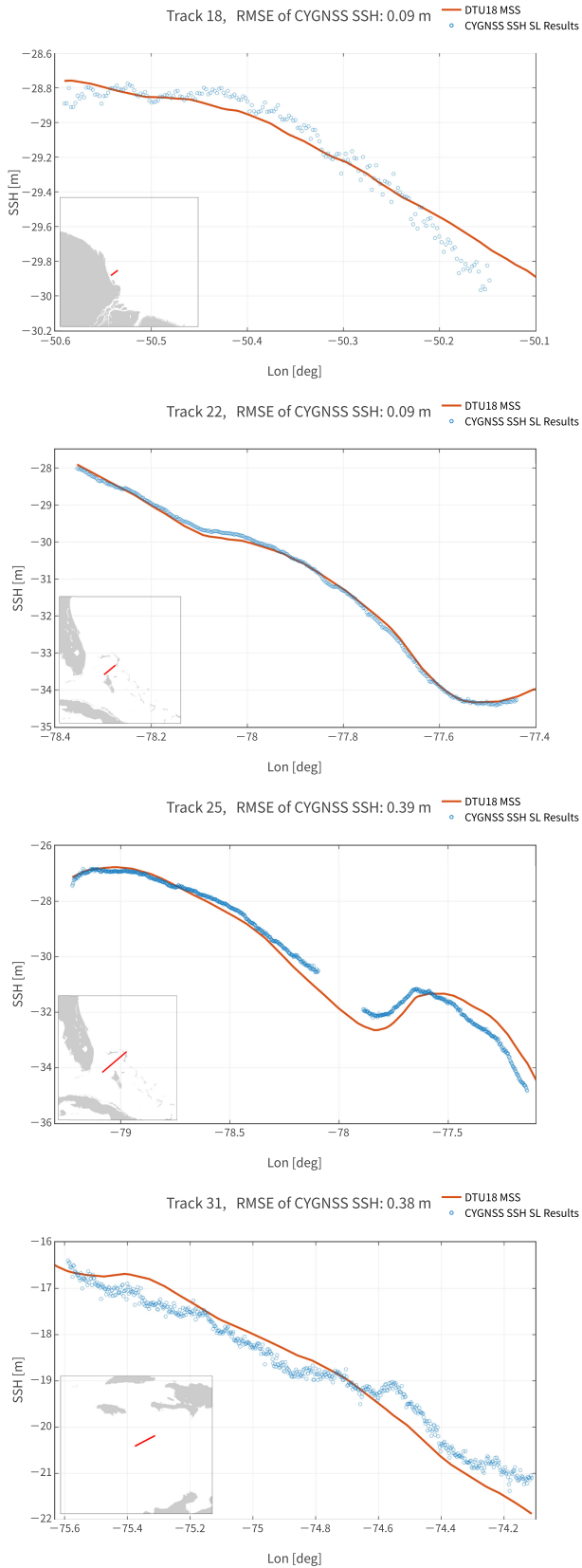


Fig. 5. Altimetric GA CaPA solutions for tracks 18, 22, 25, and 31 (top to bottom, respectively).

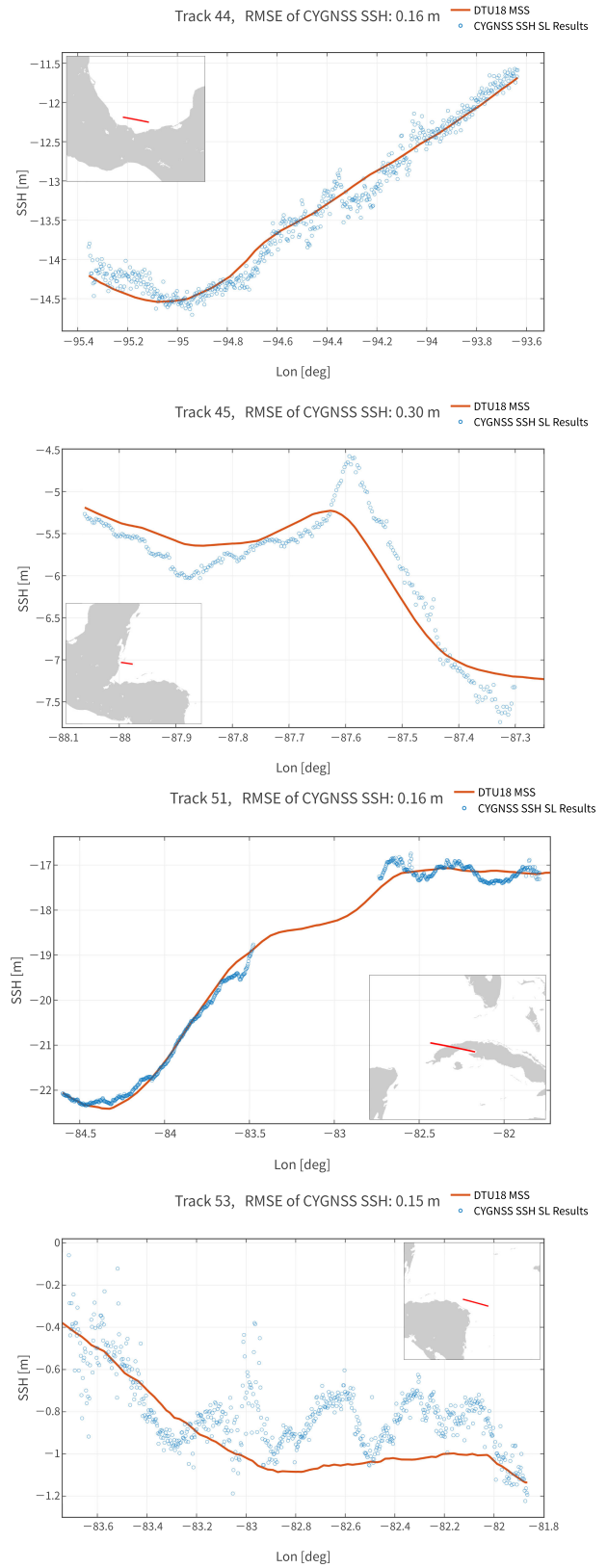


Fig. 6. Altimetric GA CaPA solutions for tracks 44, 45, 51, and 53 (top to bottom, respectively). The sharp peak in the GNSS-R solution of track 45 corresponds to the reef by the Island of Jovanni Joseph.



APPENDIX C  
COPERNICUS CLIMATE CHANGE SERVICE (C3S) CLIMATE DATA  
STORE (CDS) TOOLBOX CODE

Fig. 3 has been generated using C3S CDS Toolbox, which allows the users to analyze large amounts of climatology data without need to download them. Fig. 3 is extracted from hourly ERA-5 reanalysis data corresponding to a full year (2012), originally gridded at  $0.25^\circ \times 0.25^\circ$  cells ( $\sim 90$  GB of data). The wind and significant wave height values are first averaged to  $3 \times 3$  grid points, equivalent to  $0.75^\circ \times 0.75^\circ$  cells. The thresholds for “required calm conditions” are then applied ( $< 6$  m/s wind speed and  $< 1.5$  m SWH), and finally the number of hours during which these conditions were fulfilled are accumulated for the whole year. The results are given in percentage of the year. The CDS Toolbox runs the scripts prepared by the users, locally at ECMWF servers. The script used to generate the data for Fig. 3 is provided as follows:

```
import cdstoolbox as ct
@ct.application(title='Threshold exceedance count')
@ct.output.dataarray()
def exceedance():
    """
    Application main steps:
    -extract u, v and swh from ERA5
    for a defined time interval
    -calculate wind speed from u and v
    -define two indices which are eq
    to 1 if a condition is met and 0
    otherwise
    -multiply the indices and sum the
    file up over the time dimension
    -normalise the index to return
    percentage value
    -output the file as a NetCDF
    """
    wind_threshold = 6 #m/s
    wave_threshold = 1.5 #m
    year = ['2012']
    month = [
        '01,' '02,' '03,' '04,'
        '05,' '06,'
        '07,' '08,' '09,' '10,'
        '11,' '12'
    ]
    day = [
        '01,' '02,' '03,' '04,'
        '05,' '06,'
        '07,' '08,' '09,' '10,'
        '11,' '12,'
        '13,' '14,' '15,' '16,'
        '17,' '18,'
        '19,' '20,' '21,' '22,'
        '23,' '24,'
        '25,' '26,' '27,' '28,'
        '29,' '30,'
        '31'
    ]
    time = [
        '00:00,"01:00,"02:00,'
        '03:00,"04:00,"05:00,'
        '06:00,"07:00,"08:00,'
        '09:00,"10:00,"11:00,'
        '12:00,"13:00,"14:00,'
        '15:00,"16:00,"17:00,'
        '18:00,"19:00,"20:00,'
        '21:00,"22:00,"23:00'
    ]
    grid = ['3,' '3']
    data_u = ct.catalogue.retrieve(
        'reanalysis-era5-single-levels,'
        {
            'variable': '10m_u_component_of_wind,'
            'grid': grid,
            'product_type': 'reanalysis,'
            'year': year,
            'month': month,
            'day': day,
            'time': time,
        }
    )
    data_v= ct.catalogue.retrieve(
        'reanalysis-era5-single-levels,'
        {
            'variable': '10m_v_component_of_wind,'
            'grid': grid,
            'product_type': 'reanalysis,'
            'year': year,
            'month': month,
            'day': day,
            'time': time,
        }
    )
    data_wave = ct.catalogue.retrieve(
        'reanalysis-era5-single-levels,'
        {
            'variable': 'significant_height_of_combined_wind_waves_and_swell,'
            'grid': grid,
            'product_type': 'reanalysis,'
            'year': year,
            'month': month,
            'day': day,
```

```

        'time': time,
    }
)
wind = ct.math.sqrt((data_u)*(data_u)
+ (data_v)*(data_v))
index_wind = ct.cube.where(wind
< wind_threshold, x=1, y=0)
index_wave = ct.cube.where(data_
wave < wave_threshold, x=1, y=0)
index = ct.cube.sum((index_wave
* index_wind), 'time')
normalised_index = index/87.600
#/hours in a year and *100
(percentage)
return(normalised_index)

```

#### ACKNOWLEDGMENT

This study used NASA CyGNSS data available to the extended science team. Their GA complex waveforms are available at the ICE-CSIC/IEEC GOLD-RTR MINING server ([https://www.ice.csic.es/research/gold\\_rtr\\_mining/index.php](https://www.ice.csic.es/research/gold_rtr_mining/index.php)). The sea surface conditions were obtained from ECMWF ERA-5 products, available at the Copernicus Climate Data Store (<https://cds.climate.copernicus.eu/#!/home>). The ionospheric corrections were conducted using the IRI model (<http://irimodel.org/>) and the GIM model (<ftp://cddis.gsfc.nasa.gov/gnss/products/ionex/>). The GNSS orbits and clocks products were obtained from <ftp://ftp.gfz-potsdam.de/GNSS/products/mgex/>. DTU18 data are available at <ftp.space.dtu.dk/pub/Altimetry/FAMOS/DTU18>.

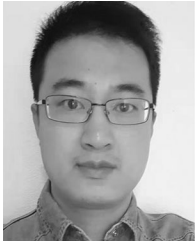
#### REFERENCES

- [1] M. P. Clarizia, C. Ruf, P. Cipollini, and C. Zuffada, "First spaceborne observation of sea surface height using GPS-reflectometry," *Geophys. Res. Lett.*, vol. 43, no. 2, pp. 767–774, 2016. [Online]. Available: <https://agupubs.onlinelibrary.wiley.com/doi/abs/10.1002/2015GL066624>
- [2] W. Li, E. Cardellach, F. Fabra, S. Ribó, and A. Rius, "Assessment of spaceborne GNSS-R ocean altimetry performance using CYGNSS mission raw data," *IEEE Trans. Geosci. Remote Sens.*, Sep. 2019, doi: [10.1109/TGRS.2019.2936108](https://doi.org/10.1109/TGRS.2019.2936108).
- [3] C. S. Ruf *et al.*, "New ocean winds satellite mission to probe hurricanes and tropical convection," *Bull. Amer. Meteorol. Soc.*, vol. 97, no. 3, pp. 385–395, 2016.
- [4] M. Unwin, P. Jales, J. Tye, C. Gommenginger, G. Foti, and J. Rosello, "Spaceborne GNSS-reflectometry on TechDemoSat-1: Early mission operations and exploitation," *IEEE J. Sel. Topics Appl. Earth Observ. Remote Sens.*, vol. 9, no. 10, pp. 4525–4539, Oct. 2016.
- [5] M. Martín-Neira, "A passive reflectometry and interferometry system (PARIS): Application to ocean altimetry," *ESA J.*, vol. 17, no. 4, pp. 331–355, 1993.
- [6] M. Martín-Neira, S. D'Addio, C. Buck, N. Floury, and R. Prieto-Cerdeira, "The PARIS ocean altimeter in-orbit demonstrator," *IEEE Trans. Geosci. Remote Sens.*, vol. 49, no. 6, pp. 2209–2237, Jun. 2011.
- [7] S. D'Addio and M. Martín-Neira, "Comparison of processing techniques for remote sensing of earth-exploiting reflected radio-navigation signals," *Electron. Lett.*, vol. 49, no. 4, pp. 292–293, Feb. 2013.
- [8] E. Cardellach *et al.*, "Consolidating the precision of interferometric GNSS-R ocean altimetry using airborne experimental data," *IEEE Trans. Geosci. Remote Sens.*, vol. 52, no. 8, pp. 4992–5004, Aug. 2014.
- [9] F. Martín, A. Camps, H. Park, S. D'Addio, M. Martín-Neira, and D. Pascual, "Cross-correlation waveform analysis for conventional and interferometric GNSS-R approaches," *IEEE J. Sel. Topics Appl. Earth Observ. Remote Sens.*, vol. 7, no. 5, pp. 1560–1572, May 2014.
- [10] A. Camps, H. Park, I. Sekulic, and J. M. Rius, "GNSS-R altimetry performance analysis for the Geros experiment on board the international space station," *Sensors*, vol. 17, no. 7, p. 1583, 2017, doi: [10.3390/s17071583](https://doi.org/10.3390/s17071583).
- [11] W. Li, A. Rius, F. Fabra, E. Cardellach, S. Ribó, and M. Martín-Neira, "Revisiting the GNSS-R waveform statistics and its impact on altimetric retrievals," *IEEE Trans. Geosci. Remote Sens.*, vol. 56, no. 5, pp. 2854–2871, May 2018.
- [12] E. Cardellach, C. Ao, M. D. la Torre Juárez, and G. Hajj, "Carrier phase delay altimetry with GPS-reflection/occultation interferometry from low earth orbiters," *Geophys. Res. Lett.*, vol. 31, no. 10, 2004, Art. no. L10402.
- [13] W. Li, E. Cardellach, F. Fabra, A. Rius, S. Ribó, and M. Martín-Neira, "First spaceborne phase altimetry over sea ice using TechDemoSat-1 GNSS-R signals," *Geophys. Res. Lett.*, vol. 44, no. 16, pp. 8369–8376, 2017.
- [14] W. Li, E. Cardellach, F. Fabra, S. Ribó, and A. Rius, "Lake level and surface topography measured with spaceborne GNSS-reflectometry from CYGNSS Mission: Example for the lake Qinghai," *Geophys. Res. Lett.*, vol. 45, no. 24, pp. 13332–13341, 2018. [Online]. Available: <https://agupubs.onlinelibrary.wiley.com/doi/abs/10.1029/2018GL080976>
- [15] A. Semmling *et al.*, "On the retrieval of the specular reflection in GNSS carrier observations for ocean altimetry," *Radio Sci.*, vol. 47, 2012, Art. no. RS6007.
- [16] J. M. Aparicio, E. Cardellach, and H. Rodríguez, "Information content in reflected signals during GPS radio occultation observations," *Atmos. Meas. Techn.*, vol. 11, no. 4, pp. 1883–1900, 2018. [Online]. Available: <https://www.atmos-meas-tech.net/11/1883/2018/>
- [17] G. Beyerle, K. Hocke, J. Wickert, T. Schmidt, C. Marquardt, and C. Reigber, "GPS radio occultations with CHAMP: A radio holographic analysis of GPS signal propagation in the troposphere and surface reflections," *J. Geophys. Res., Atmos.*, vol. 107, no. D24, pp. ACL 27-1–ACL 27-14, 2002. [Online]. Available: <https://agupubs.onlinelibrary.wiley.com/doi/abs/10.1029/2001JD001402>
- [18] A. Semmling *et al.*, "Sea surface topography retrieved from GNSS reflectometry phase data of the GEOHALO flight mission," *Geophys. Res. Lett.*, vol. 41, no. 3, pp. 954–960, 2014.
- [19] "ERA5: Fifth generation of ECMWF atmospheric reanalyses of the global climate," Copernicus Climate Change Service Climate Data Store, 2017. [Online]. Available: <https://cds.climate.copernicus.eu/cdsapp#!/home>. Accessed on: Jun. 4, 2019.
- [20] C. M. Ho, B. D. Wilson, A. J. Mannucci, U. J. Lindqwister, and D. N. Yuan, "A comparative study of ionospheric total electron content measurements using global ionospheric maps of GPS, TOPEX radar, and the Bent model," *Radio Sci.*, vol. 32, no. 4, pp. 1499–1512, Jul. 1997.
- [21] J. Wickert *et al.*, "GEROS-ISS: GNSS reflectometry, radio occultation, and scatterometry onboard the international space station," *IEEE J. Sel. Topics Appl. Earth Observ. Remote Sens.*, vol. 9, no. 10, pp. 4552–4581, Oct. 2016.
- [22] E. Cardellach *et al.*, "GNSS transpolar earth reflectometry exploring system (G-TERN): Mission concept," *IEEE Access*, vol. 6, pp. 13980–14018, 2018.
- [23] F. Zus *et al.*, "A methodology to compute GPS slant total delays in a numerical weather model," *Radio Sci.*, vol. 47, no. 2, 2012, Art. no. RS2018. [Online]. Available: <https://agupubs.onlinelibrary.wiley.com/doi/abs/10.1029/2011RS004853>
- [24] D. Bilitza *et al.*, "The international reference ionosphere today and in the future," *J. Geodesy*, vol. 85, pp. 909–920, 2011.
- [25] D. Wingham *et al.*, "CryoSat: A mission to determine the fluctuations in earth's land and marine ice fields," *Adv. Space Res.*, vol. 37, pp. 841–871, 2006.
- [26] V. Kudryavtsev, A. Monzikova, C. Combot, B. Chapron, N. Reul, and Y. Quilfen, "A simplified model for the baroclinic and barotropic ocean response to moving tropical cyclones: 1. Satellite observations," *J. Geophys. Res., Oceans*, vol. 124, no. 5, pp. 3446–3461, 2019. [Online]. Available: <https://agupubs.onlinelibrary.wiley.com/doi/abs/10.1029/2018JC014746>
- [27] L.-L. Fu and C. Ubelmann, "On the transition from profile altimeter to swath altimeter for observing global ocean surface topography," *J. Atmos. Ocean. Technol.*, vol. 31, no. 2, pp. 560–568, 2014. [Online]. Available: <https://doi.org/10.1175/JTECH-D-13-00109.1>



**Estel Cardellach** (Senior Member, IEEE) received the Ph.D. degree in physics from the Polytechnic University of Catalonia, Barcelona, Spain, in 2002.

She has been involved in scientific applications of Global Navigation Satellite Systems (GNSS) for remote sensing of the earth, such as the extraction of geophysical information of the GNSS reflected signals, radio occultation, and geodetic techniques. She was a Postdoc with the NASA/Jet Propulsion Laboratory, Pasadena, CA, USA (2003), and with the Harvard Smithsonian Center for Astrophysics, Cambridge, MA, USA (2004). Since 2005, she has been with the Institute of Space Sciences (ICE-CSIC/IEEC), Barcelona, Spain. She was a Co-Chair of the Science Advisory Group of ESA's GEROS-ISS mission, and a Co-Principal Investigator of the G-TERN proposal, in response to ESA EE9 mission call. She is currently the Principal Investigator of the spaceborne experiment Radio Occultation and Heavy Precipitation aboard the PAZ low earth orbiter.



**Weiqiang Li** (Member, IEEE) received the B.S. degree in electronic engineering and Ph.D. degree in communication and information system from Beihang University, Beijing, China, in 2004 and 2012, respectively.

His Ph.D. thesis was on the signal processing methods and instrumentation of the earth reflected Global Navigation Satellite Systems (GNSS) signal for remote sensing purposes. Since 2014, he has been with the Earth Observation Research Group, Institute of Space Sciences (ICE-CSIC/IEEC), Barcelona, Spain,

working on geophysical applications of GNSS.



**Antonio Rius** received the Ph.D. degree from Barcelona University, Barcelona, Spain, in 1974.

From 1975 to 1985, he was a member of the Technical Staff at NASA's Deep Space Communications Complex, Madrid, Spain, where he was responsible for the radio astronomical activities. Since 1986, he has been with the Spanish Research Council (CSIC), Madrid, Spain. He is currently a CSIC Research Professor AH with the Research Group on Earth Observation, Institut d'Estudis Espacials de Catalunya, Barcelona, Spain.



**Maximilian Semmling** received the degree in physics from Leipzig University, Leipzig, Germany, in 2007 and the Ph.D. degree in natural sciences, geodesy and geoinformation science from the Technical University of Berlin, Berlin, Germany, in 2012.

Since 2008, he has been with the Department of Geodesy, GeoForschungsZentrum, Potsdam, Germany. He is experienced in ground-based experiments for sea ice reflectometry in the Arctic, airborne experiments for sea surface altimetry with a Zeppelin airship over Lake Constance, and with the high altitude long

range research aircraft over the Mediterranean Sea. He was a member of the GEROS-ISS team, working on its phase altimetry aspects. His research interests include the field of Global Navigation Satellite Systems reflectometry and its application for remote sensing.



**Jens Wickert** received the graduate degree in physics from the Technische Universität Dresden, Dresden, Germany, in 1989 and the Ph.D. degree in geophysics/meteorology from the University of Graz, Graz, Austria, in 2002.

He worked for several institutions as AWI, DLR, and DWD before he joined GeoForschungsZentrum in 1999. He is currently a Research Topic Director "Atmosphere in Global Change," Deputy Section Head of the Space Geodetic Techniques, and Head of the Research Area Global Navigation Satellite Systems (GNSS) Remote Sensing. Since 2016, he has been a Professor of GNSS Remote Sensing and Positioning with the Technische Universität Berlin, Berlin, Germany. He is involved in numerous interdisciplinary GNSS related research projects. He was a Principal Investigator of the pioneering GPS Radio Occultation experiment aboard the German CHAMP satellite. He was also coordinating the GEROS-ISS proposal to ESA and chairing the related Science Advisory Group. He was a Co-PI of the G-TERN Earth Explorer 9 proposal and is the author/co-author of more than 230 ISI listed publications on GNSS Earth Observation.



**Florian Zus** received the Technical Physics degree from Graz University of Technology, Graz, Austria, and the Ph.D. degree in physics/meteorology from the University of Hohenheim, Stuttgart, Germany, in 2003 and 2010, respectively.

He is currently with the German Research Center for Geosciences, Potsdam, Germany, working in the field of atmospheric remote sensing with the Global Navigation Satellite System.



**Christopher S. Ruf** (Fellow, IEEE) received the B.A. degree in physics from Reed College, Portland, OR, USA, in 1982, and the Ph.D. degree in electrical and computer engineering from the University of Massachusetts, Amherst, MA, USA, in 1987.

He is currently the Frederick Bartman Collegiate Professor of Climate and Space Science with the University of Michigan, Ann Arbor, MI, USA, and the Principal Investigator of the Cyclone Global Navigation Satellite System (GNSS) NASA Earth Venture mission. He was with Intel Corporation, Hughes Space and Communication, the NASA Jet Propulsion Laboratory, and Penn State University. His research interests include GNSS-R remote sensing, microwave radiometry, atmosphere and ocean geophysical retrieval algorithm development, and sensor technology development.

Dr. Ruf is a member of the American Geophysical Union, the American Meteorological Society, and Commission F of the Union Radio Scientifique Internationale. He is a former Editor-in-Chief for the IEEE TRANSACTIONS ON GEOSCIENCE AND REMOTE SENSING and was on the editorial boards of *Radio Science* and the *Journal of Atmospheric and Oceanic Technology*. He is the recipient of four NASA Certificates of Recognition and seven NASA Group Achievement Awards, as well as the 1997 TGRS Best Paper Award, the 1999 IEEE Resnik Technical Field Award, the 2006 IGARSS Best Paper Award, and the 2014 IEEE GRSS-S Outstanding Service Award.



**Carlo Buontempo** received the Ph.D. degree in physics from the University of L'Aquila, L'Aquila, Italy, in 2004, with a thesis on the interaction between troposphere and stratosphere in the tropics.

Then, he moved to York University, Toronto, ON, Canada, for a Postdoc on the role of convection in controlling the distribution of trace gases in the upper troposphere. In 2005, he joined the Met Office Hadley Centre for almost a decade, where he led the climate adaptation team and the climate service development team. He is currently a Deputy Director of the Copernicus Climate Change Service with the European Centre for Medium-Range Weather Forecasts, Reading, U.K., where he also manages its sectoral information system.